IUTAM Symposium on Dynamics of Capsules, Vesicles and Cells in Flow

Static response of coated microbubbles: Modeling simulations and parameter estimation

Alkmini Lytra[a], Nikos Pelekasis[a]*, Vassilis Sboros[b], Emmanouil Glynos[c], Vasileios Koutsos[d]

[a]*Department of Mechanical Engineering, University of Thessaly, Volos 38334, Greece*
[b]*School of Engineering, Heriot Watt University, Edinburgh, EH14, 4AS, United Kindom*
[c]*Department of Materials Science and Engineering, Biointerfaces Institute, University of Michigan, Ann Arbor, Michigan 48109, United States*
[d]*Insitute for Materials and Processes, School of Engineering, The University of Edinburgh, Edinburgh, EH9 3JL, United Kingdom*

Abstract

The mechanical response of contrast agent microbubbles subject to a static load was investigated in force-deformation curves. Asymptotic relations are fitted in available from literature experimental AFM measurements of polymeric microbubbles. The elastic modulus and shell thickness are estimated based on the transition from the classical linear (Reissner) to the nonlinear (Pogorelov) regime. The estimated value of the elastic modulus is in the order of GPa and the shell thickness in the order of nm, in good agreement with independent estimates. Numerical simulations recover the above transition and identify a third regime, dominated by the compressibility of the enclosed gas.

1. Introduction

Contrast agents are microbubbles enclosed by a viscoelastic shell. The material of the shell can store elastic energy thus providing mechanical strength to the microbubbles[1]. Moreover, the lifetime of a contrast agent is several times greater than the lifetime of a free microbubble into the water[1] because the gas dissolution process is decelerated. The shell is considered as an elastic solid that deforms under the action of external forces. Polymers or

* Corresponding author. Tel.: 0030-24210-74102
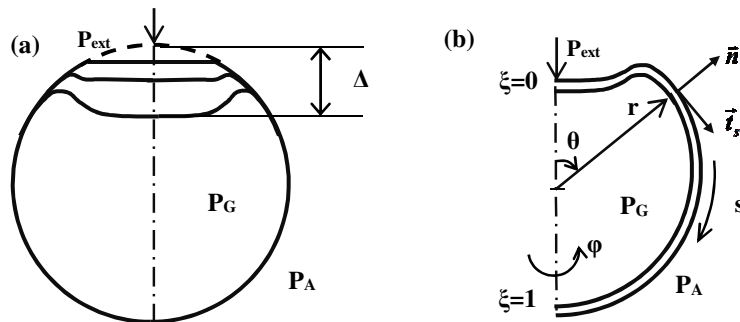 *E-mail address:* pel@uth.gr

phospholipids

Fig. 1 (a) Deformed bubble subject to an increasing static point load, (b) lagrangian representation.

usually construct the shell. The former are harder than phospholipids[2,3,4] in terms of their elastic modulus. Their mechanical strength enables them to be excellent drug/ gene carriers through arteries or contrast enhancers via ultrasound[5]. Accurate estimation of their elastic properties is a key to design and predict their response in biological tubes or tissues. The present work aims at developing a new tool to estimate the elastic modulus and thickness of shell coatings, combining available experimental measurements[3], theoretical relations and numerical modeling.

In particular, Glynos et al.[3] have investigated the response of biSphere microbubbles employing atomic force microscopy (AFM), which can perform accurate measurements of force and deformation of the microbubbles. These microbubbles consist of a stiff polylactide shell surrounded by a thin (~10 nm) layer of cross-linked albumin outer layer to make the MS harmless to the human body. The analysis of Glynos et al. contains an extensive number of force-deformation curves (to be referred to as f-d curves in the following for brevity) using various cantilever stiffnesses. Three different regimes were observed in the f-d curves, see Fig. 2. The f-d curves exhibit an initial short nonlinear [6,7,8] regime up to about 10 nm and 10 nN pertaining to the cross-linked albumin outer layer, denoted with 1 in Fig. 2. Then an extensive linear regime (denoted with 2) is observed where the elastic forces originating from the stiff polylactide layer are dominant[9]. The linear regime is followed by a nonlinear[10,11], but curved downwards regime (3). Finally, at large enough deformations the f-d curve exhibits a fourth regime which is slightly curved upwards, indicating the effect of gas compressibility on the composite stiffness of the microbubble. This regime becomes mostly evident when soft phospholipid shells are examined by AFM[2].

Detection and verification of the above force regimes is essential for estimating the elastic properties of the shell, in particular the elastic modulus (E) and shell thickness (h) as shown in section 3 below, upon combining the experimental curves with the appropriate asymptotic relations describing the dominant force balances. For example, Reissner[9] and Pogorelov[10] theories describe the balance between stretching and bending within the linear and nonlinear regions, respectively, of the f-d curves discussed above. The novelty of this work lies in the fact that we can estimate both shell thickness and Young's modulus without prior knowledge of the thickness, especially for polymeric shells, by exploiting the above theories[9,10] describing transition from the linear to the nonlinear regime of the static response curve. Phospholipid shells are much softer than polylactide shells and start deforming at much smaller forces[2]. Furthermore, they are affected by gas compressibility for a much lower force range, in comparison with the hard polymeric shells, at large deformations[12]. Hence, the effect of intermolecular/adhesion forces and compressibility have to be accounted for in order to obtain reliable estimates of their elastic properties. Consequently, the present study implements the above described novel approach mainly to the case of polymeric shells, leaving a more complete analysis that would be relevant to phospholipid shells to a future study. In the present study we have developed a numerical model based on finite elements in order to simulate the mechanical response to static loading and recover three of the above four regimes in the f-d curves; the first nonlinear regime

where intermolecular forces dominate is not captured. The microbubble is considered as an axisymmetric shell[13] subject to a point force at the one pole whereas the gas that is encapsulated in the microbubble is assumed to undergo isothermal compression. The shell properties are provided by employing asymptotic relations from the literature[9,10] in order to fit the linear and nonlinear regimes of experimentally obtained f-d curves[3]. The normal and tangential
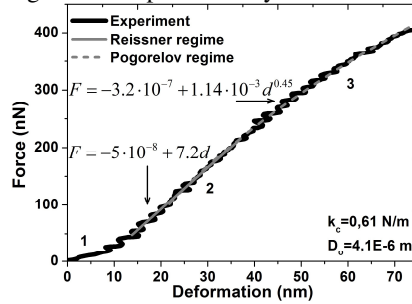

Fig. 2 Experimental force-deformation curve[3].

force balances are employed on the microbubble shell, including elastic and external pressure forces coupled with the isothermal expansion for the enclosed gas, in order to solve for the spherical coordinates, r,θ, of the deformed shell and the internal gas pressure, P_G. As part of the post-processing, we can calculate the energies (bending and stretching) that are stored in the elastic shell as well as the energy due to gas compressibility. In section 2, an extensive discussion is presented regarding the problem formulation and the numerical methodology. In section 3, the asymptotic relations are fitted in experimental curves in order to estimate the elastic modulus and the thickness of the shell and numerical results are compared against experimental measurements[3] in the form of f-d curves. Finally, in section 4 the main conclusions of the present work are outlined.

2. Theoretical modeling, numerical implementation and validation

The static response of a microbubble, Fig. 1(b), subject to external point load is studied in order to investigate (a) the f-d curve, (b) the energies that are stored in the shell or in the encapsulated gas and (c) the shape of the shell in the deformed configuration. The microbubble is considered as an axisymmetric shell, where every particle (ξ) along the interface is described by the normal and tangential unit vectors, see also Fig. 1(b),

$$\vec{n} = \left(r\theta_\xi \vec{e}_r - r_\xi \vec{e}_\theta \right)/s_\xi , \qquad \vec{t}_s = \left(r_\xi \vec{e}_r + r\theta_\xi \vec{e}_\theta \right)/s_\xi , \qquad \vec{t}_\varphi = r\sin\theta \vec{e}_\varphi , \qquad s_\xi = \left(r_\xi^2 + r^2\theta_\xi^2 \right)^{0.5} \qquad (1)$$

where, r, θ and φ are spherical radial, polar and azimuthal coordinates, respectively, s is the arc-length along the meridian and ξ denotes Lagrangian particles on the interface; when used as subscript ξ signifies differentiation. The normal and tangential components of the force balance on the interface assume the form[13,14,15,16]:

$$\Delta\vec{F} = \Delta F\vec{n} + \Delta F\vec{e}_s = -\vec{\nabla}_s \cdot \underline{\underline{T}} = \Delta P\vec{n}$$

$$\underline{\underline{T}} = \underline{\underline{\tau}} + \vec{q}\vec{n}, \qquad \underline{\underline{\tau}} = \tau_s \vec{e}_s \vec{e}_s + \tau_\varphi \vec{e}_\varphi \vec{e}_\varphi, \qquad \vec{q} = q\vec{e}_s, \qquad \Delta P = \begin{cases} P_{ext} + P_A - P_G & ,\xi = 0 \\ P_A - P_G & ,\xi \neq 0 \end{cases} \qquad (2a)$$

where $\vec{\nabla}_s$ is the surface gradient operator, T the tension tensor, τ the elastic tensor and P_{ext}, P_A, P_G are the applied point load, atmospheric and gas pressure, respectively. A torque balance on an infinitesimal interfacial patch relates the normal shear stress q with the bending moment m tensor:

$$\vec{q} = \vec{\nabla}_s \cdot \underline{\underline{m}} \cdot \left(\underline{I} - \vec{n}\vec{n} \right), \qquad \underline{\underline{m}} = m_s \vec{e}_s \vec{e}_s + m_\varphi \vec{e}_\varphi \vec{e}_\varphi, \qquad m_i = k_b \left(K_i + \nu K_j \right) \big/ \lambda_j, \qquad K_i \equiv \lambda_i k_i - k_i^R \tag{2b}$$

$$k_b = Eh^3 \big/ 12 \left(1 - \nu^2 \right), \qquad \lambda_i = ds_i \big/ dS_i \quad i, j = s \text{ or } \varphi \quad i \neq j \text{ indices are not summed} \tag{2c}$$

where k_b is the bending modulus, K_i are the bending strains along the principal directions of the interface, k_i signifies the principal curvature (superscript R denotes the reference state) and ds_i and dS_i indicate infinitesimal lengths in the principal directions of deformed and undeformed configurations, respectively. Substituting the above equations into the normal and tangential force balance we obtain:

$$\Delta F_n = k_s \tau_s + k_\varphi \tau_\varphi - \frac{1}{\sigma} \frac{\partial (\sigma q)}{\partial s} = \Delta P, \qquad \Delta F_s = - \left(\frac{\partial \tau_{ss}}{\partial s} + \frac{1}{\sigma} \frac{\partial \sigma}{\partial s} \left(\tau_s - \tau_\varphi \right) + k_s q \right) = 0$$

$$q = \frac{1}{\sigma} \frac{\partial \sigma}{\partial s} \left(\frac{\partial (\sigma m_s)}{\partial \sigma} - m_\varphi \right), \qquad \sigma = r \sin \theta \tag{3}$$

The resultant strains are related to stresses with the linear neo-Hookean constitutive law[17]:

$$\tau = G_s \frac{1+\nu}{1-\nu} \left(\lambda^2 - 1 \right) \tag{4}$$

with G_s the surface shear modulus and ν the Poisson ratio. The gas encapsulated in the bubble is treated as an ideal gas undergoing isothermal compression. Then pressure and volume variations of the enclosed gas are related via:

$$P_G V_f = P_A V_i \tag{5}$$

with indices f and i indicating the bubble volume in the final and initial stage, respectively. The initial gas pressure is assumed to be equal to the atmospheric pressure P_A corresponding to the shell being at a stress free state. Moreover, the center of mass of the microbubble is set to zero, in order to avoid any solution related to rigid body motion. This assumption is realistic since in the AFM experiment -that this model simulates- the microbubble remains at the same position for every applied load from the cantilever. During the experiment the microbubble is also subject to an equal force from the substrate supporting it that causes a similar deformation in the bottom part of the shell. However, the calculation in the present study focuses on the deformation of the top portion of the shell, which is the one associated with the actual measurement, and is not affected by the load in the bottom. Thus, the component of the center of mass along the axis of symmetry, z_{cm}, is set to zero:

$$z_{cm} = \frac{1}{V} \iiint_V \vec{r} \cdot \vec{e}_z dV = 0 \tag{6}$$

The system of the above equations (3-6) is completed with the following symmetry conditions at the two poles signified by Lagrangian particles $\xi = 0$ and $\xi = 1$:

$$r_\xi = \theta_{\xi\xi} = 0, \qquad \text{at} \qquad \xi = 0 \quad \& \quad 1 \tag{7}$$

Furthermore, the shell can store elastic energy (stretching and bending), since it consists of an elastic material. When a neo-Hookean constitutive law is considered the stretching and bending energy are:

$$E_s = \frac{G_s}{2(1-v^2)} \int\limits_{A_o} \left(e_s^2 + 2v e_s e_\varphi + e_\varphi^2 \right) dA_o, \qquad e_i = \frac{1}{2}\left(\lambda_i^2 - 1\right) \tag{8a}$$

$$E_b = \frac{k_b}{2} \int\limits_{A_o} \left(K_s^2 + 2v K_s K_\varphi + K_\varphi^2 \right) dA_o \tag{8b}$$

where A_o denotes the undeformed area of the shell and e_i are the principal strains.

The energy due to changes of pressure and volume of the compressible gas that is encapsulated into the elastic shell is called gas compression energy and is related to the work that is consumed to overcome the internal pressure (P_G):

$$E_c = -P_A V_o \ln\left(V_f / V_i\right) + P_A \left(V_f - V_i\right) \tag{8c}$$

Calculation of the above energies gives an excellent tool to describe the dominant resistance to shell deformation (stretching, bending or compression) that is most important in identifying the nature of every solution, as shown below. Finally, the formulation of the problem is completed by writing the equations in dimensionless form. This is possible by introducing the characteristic length scale, R_o corresponding to the bubble radius at rest. Consequently, the solution of the model (r, θ, P_G) depends mainly on two dimensionless parameters:

$$\tilde{k}_b = \frac{k_b}{\chi R_o^2} = \left(\frac{h}{3R_0}\right)^2, \qquad \tilde{P} = \frac{P_A R_o}{\chi}, \qquad \chi \equiv Eh \tag{9}$$

where $\chi = Eh$ is the area dilatation modulus. The first parameter (dimensionless bending modulus) is defined as the ratio of bending resistance to stretching resistance, while the second (dimensionless pressure) measures the ratio of resistance to gas compression to the resistance to stretching. Therefore, the above parameters quantify the relative importance among these different sources of stiffness for given loading conditions. Thus, for example the normal component of force balance reads in dimensionless form and spherical coordinates as:

$$\tilde{P}_{ext} = \left(\tilde{P}_G - \tilde{P}_A\right) - \left(k_s \tau_s + k_\varphi \tau_\varphi\right) + \frac{1}{\sigma}\frac{d}{ds}\left(\frac{d\sigma}{ds}\left(\frac{d\left(\sigma m_s\right)}{d\sigma} - m_\varphi\right)\right) \tag{10}$$

illustrating the fact that the applied force from the AFM balances the resistance due to compression, elongation and bending signified by the three terms in parentheses; in the above eq. parameter $\tilde{k}_b$ is contained in the dimensionless form of the bending moments, m_s, m_φ.

The normal and tangential force balances coupled with the isothermal ideal gas compression law, are discretized with the finite element methodology in order to capture the displaced Lagrangian particles in terms of their spherical coordinates, r & θ, along the generating curve of the axisymmetric shell. Moreover, one of the equations corresponding to the tangential force balance is replaced by the equation that fixes the center of mass, eq. (6), in order to avoid any net translational motion of the shell along the axis of symmetry, see also the relevant discussion in the previous section. The unknown Lagrangian particle positions are written as a function of a number of B-cubic spline polynomials[18]:

$$r\left(\xi\right) = \sum_{i=0}^{N+1} a_i B_i \qquad \text{and} \qquad \theta\left(\xi\right) = \sum_{i=0}^{N+1} b_i B_i \tag{11}$$

where N denotes the number of nodes along the discretized domain and a_i, b_i are the unknown coefficients. The expressions in equation (11) imply that the domain contains two imaginary nodes at the two poles ($\xi=0$ and $\xi=1$). In order to estimate the values of the corresponding unknown variables a_0, a_{N+1}, b_0 and b_{N+1}, the boundary conditions of equation (7) are applied as additional equations. The choice of B-cubic splines polynomials as basis function was based on the fact that fourth order derivatives of r and θ coordinates enter the force balance. However, after integration by parts is performed the weak form of the normal and tangential force balances contain up to 2nd and 3rd order derivatives, respectively; e.g. the normal force balance assumes the form:

$$\int_0^1 \left(\left(\tilde{P}_{ext} + \tilde{P}_A - \tilde{P}_G + k_s \tau_s + k_\varphi \tau_\varphi \right) B_i s_\xi r \sin\theta - \left(B_{i,\xi} \sigma_\xi m_\varphi / s_\xi + \sigma m_s \left(B_{i,\xi} / s_\xi \right)_\xi \right) \right) d\xi = 0 \tag{12}$$

Consequently, since cubic splines guarantee continuity up to the 2nd derivative[19] the above weak formulation is valid. The equations of isothermal gas compression and the position of the center of mass are written in their integral form:

$$\tilde{P}_{atm} - \tilde{P}_G \int_0^1 0.5 r^3 \theta_\xi \sin\theta \, d\xi = 0 \tag{13}$$

$$0.5\pi \int_0^1 r^4 \theta_\xi \cos\theta \sin\theta \, d\xi = 0 \tag{14}$$

Equations (12) - (14) can take the form of residuals:

$$R_i \left(r_j, \theta_i, P_G \right) = 0 \qquad i, j = 0, N+1 \tag{15}$$

The solution of the above system of equations is obtained using an iterative scheme in a standard Newton's algorithm. In particular, the x_i unknown variable is computed in $k+1$th iteration for a given value of the same variable at the kth iteration:

$$J_{ij} \left(x_i^k \right) \Delta x_j^k = R_i^k \left(x_i^k \right), \qquad J_{ij} = \frac{\partial R_{ij}}{\partial x_j} \approx \frac{R_i \left(x_j + \Delta x_j \right)}{\Delta x_j}, \qquad \Delta x_j^k = x_j^k - x_j^{k+1} \tag{16}$$

where J denotes the Jacobian matrix and x is a vector which contains the unknown coefficients and the internal pressure P_G, $\vec{x} = (\alpha_i, b_i, P_G)^T$. Moreover, the complexity of the integrals, especially in the normal and tangential force balances, doesn't allow for an analytical calculation of the derivatives in the Jacobian matrix. In order to avoid multiple solutions, the first derivative of every residual in equation (12) is computed numerically with finite differences and a setting $\Delta x = 10^{-8}$. On the other hand, the Jacobian entries of residuals in equations (13) and (14) are computed analytically. The system of equations in (15) is solved by using the dgesv lapack routine. The computational domain is typically discretized by 400 elements, while a finer mesh essentially reproduces the above result. The Fortran code has been validated by calculating the critical buckling load and comparing the numerical value with the analytical expression[13] for a uniform external load. Eq. (17) for the case that is investigated in the next section gives $\Delta P_{CR} = 1.86 \cdot 10^6$ Pa, while the numerically obtained value is $1.77 \ 10^6$ Pa as depicted below in Fig. 3(a) along with the relevant bifurcation diagram. Furthermore, the behaviour of microbubbles subject to a uniform external load was previously investigated[12] and the bifurcation diagrams that were obtained were compared against those from similar studies in the literature[20] with excellent agreement.

$$\Delta P_{CR} = \frac{2E}{\sqrt{3\left(1-v^2\right)}}\left(\frac{h}{R_o}\right)^2 \tag{17}$$

As an additional test f-d curves were obtained for a point load, for the hard shell studied in Fig 3(a), Fig 3(b) with R_0=2 μm, h=31 nm and E=6.1 GPa or $\chi\approx$180 N/m, and for a soft shell, Fig 3(c), with R_0=1.5μm and χ=0.4 N/m. The resulting response curves are shown in Figs 3(b) and 3(c) clearly illustrating three among the four regimes mentioned above, except for the initial one dominated by intermolecular forces. The appearance of the linear Reissner followed by the nonlinear Pogorelov regime, with the corresponding flattened and crater forming shapes, serves as an additional validation of the numerical code. The sensitivity of soft shells to pressure changes is
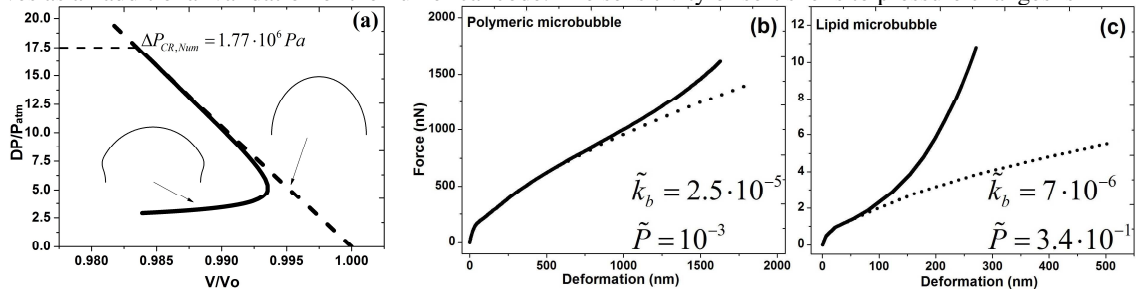

Fig. 3(a) Bifurcation diagram for a shell subject to a uniform external load; R_0=2 μm, E=6.1 GPa and h=31 nm. (b) and (c) f-d curves for a polymeric and a lipid microbubble, respectively.

also illustrated by the early transition to an upward curved regime in Fig 3(c) where gas compressibility plays a central role. On the contrary, the hard shell interrogated in Fig 3(b) needs to be subjected to an unrealistically large external load before it exhibits a similar response. This was anticipated due to the much larger value of dimensionless pressure $\tilde{P}$ for the soft shell studied in Fig. 3(c). In Figs. 3(b) and (c) the two different approaches were adopted for the pressure of the encapsulated gas, i.e assuming isothermal variation (continuous curves) and constant internal pressure (dashed lines). For small deformations the two pressure models give identical results, whereas for large deformations the gas pressure in the shell increases significantly as the shell is compressed, thus contributing to the shell stiffness.

3. Results and discussion

A typical f-d curve[3] obtained via AFM measurement can be seen in Fig. 2. Three distinctly different regimes can be observed. An initial nonlinear regime, denoted with 1 in Fig. 2, occurs for very small values of the applied force, on the order of 10 nN and less, where the Albumin outer layer (thickness: ~10 nm) and intermolecular/surface-adhesion forces between the shell and the cantilever are conjectured to participate in the dominant force balance with elastic forces. As the external load increases a linear regime appears, denoted with 2, followed by a nonlinear regime, denoted by 3, that is curved downwards. The linear regime is the classical Reissner[9] regime where stretching and bending forces coming from the stiff polylactide shell balance each other over a flattened contact area that characterizes the microbubble shape. This is the part of the f-d curve that is typically used in the literature in order to infer the shell elasticity modulus once the shell thickness and radius are known[3,21]. The third regime occurs as the external load further increases and it is known in the literature as Pogorelov[10] regime; it appears as the compressive load on the flattened part of the shell exceeds a certain value, in which case the shell bents forming a crater at the pole region while a dimple forms at some distance from the pole where most of the bending energy is stored. In the present study we investigate the possibility of using both Reissner and Pogorelov regimes in order to estimate the shell elastic modulus and thickness. To this end, we fit the asymptotic relations from Reissner's[9] and Pogorelov's[10]

theory in the experimental curve, see Fig. 2, in order to obtain the slopes of the linear and nonlinear regimes, respectively:

$$\text{Reissner: } F = \frac{4}{\left(3\left(1-\nu^2\right)\right)^{0.5}} \frac{Eh^2}{R_o} \Delta, \qquad \text{Pogorelov: } F = \left(\frac{E^2 h^5}{R_o^2} \Delta\right)^{0.5} \tag{18a,b}$$

with F denoting the applied force and Δ the deformation of the shell. Through this process, as shown in Fig. 2, and setting $\nu=0.5$ we obtain for a microbubble of diameter D_o=4.1 μm:

$$F / \Delta = 7.2 \quad \& \quad F / \sqrt{\Delta} = 1.14 \cdot 10^{-3} \xrightarrow{\;eqs.(18)\;} E = 6.1 \text{ GPa and } h = 31 \text{ nm} \tag{19}$$
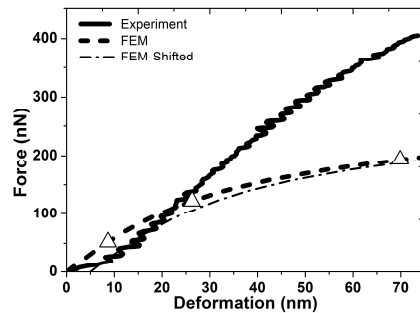

Fig. 4 Comparison between numerical and experimental results.

The above calculation of the elastic modulus (E) and the thickness (h) of the shell has been repeated for all the available experimental measurements by Glynos et al.[3], see Table 1 below. The experimental estimates of the shell elastic modulus have been obtained using two different tipless cantilevers, with stiffness k_c=0.61 N/m and 1.14 N/m. Moreover, it should be stressed that they are based on Reissner's theory, equation (18a), while adopting a linear empirical equation[3,22], h=1.5·10$^{-2}R_o$, for the shell thickness that is provided by the manufacturer. As it becomes evident from Table 1, the calculated values for the elastic modulus and shell thickness obtained by combining the Reissner and Pogorelov asymptotic relations, eqs (18a,b), are in good agreement with the experimental estimates without requiring prior knowledge of the shell thickness.

Table 1.Comparison of the values of elastic modulus (E) and thickness (h) between experiments and asymptotic analysis.

k_c=0.61 N/m	Experiment		Asymptotic eq.	
Initial diameter [μm]	E [GPa]	h [nm]	E [GPa]	h [nm]
2.6	16	20	8.5	25
3.5	7.5	26	12	26
4.1	4.5	31	6.1	31
k_c=1.14 N/m				
3.1	8	23	3.4	35
3.2	7	25	14	20
4.0	4.5	31	4.7	30
4.9	2.5	38	4.5	31
5.5	2.5	42	1.7	47

In order to validate the above picture describing the shell static response, we compare the experimental f-d curves with the ones obtained by numerical simulations, see Fig. 4, based on the model described in section 2. The

parameters of the model are provided by the methodology proposed in section 3 of the present study. In particular we study the static response to a point load of the microbubble studied in Fig. 4, with rest diameter D_o=4.1 μm and elastic properties E=6.1 GPa, h=31 nm, and v=0.5 for a shell that follows the neo-Hookean constitutive law.

As can be gleaned from Fig. 4, the numerical simulation of the static response to a point load failed to describe the first nonlinear regime, because intermolecular/surface-adhesion forces are not included in the model; compression of the thin soft gel layer introduced for biocompatibity is conjectured to also participate in the force balance in this regime. On the other hand, regimes (2) and (3) are qualitatively captured by the simulation. The transition from flattened shell shapes obtained for small external loads, typically associated with the linear Reissner regime in the f-d curve, to shapes exhibiting crater formation, associated with the nonlinear Pogorelov regime in the f-d curve, is illustrated in Fig. 5(a) for normalized deformations 0.004, 0.015 and 0.035 which correspond to points indicated by filled triangles in the numerically obtained f-d curve shown in Fig. 4. However, it should be stressed that the latter curve overestimates the deformation of the shell for the same external load. This discrepancy is attributed to the fact that the numerical model estimates the deformation of the shell exactly at the pole (ξ=0), while in the experiments the deformation is estimated based on the movement of the cantilever which will be the same as the deformation at the pole for a flattened shape in the Reissner regime but different, in fact smaller, when a crater is
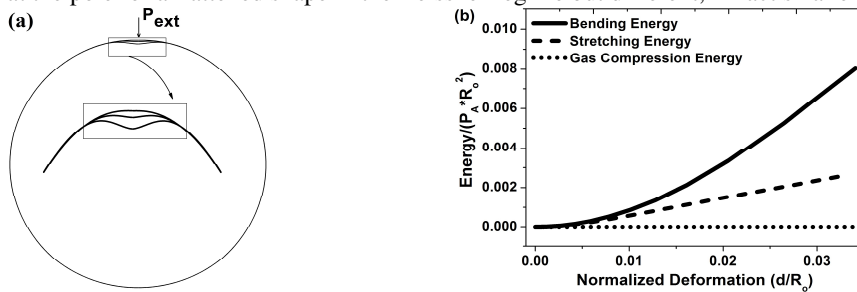

Fig. 5. Numerically obtained (a) shapes at a normalized deformation of 0.004, 0.015 and 0.035 and (b) distribution of energies

formed. Moreover, in the numerical model we use a point force, eq 2b, to describe the loading from the AFM, which is valid for small deformations. At higher deformations the contact area between microbubble and cantilever is large and the loading has a distribution along the interface. Finally, three dimensional deformations are not included in the axisymmetric numerical model, which may occur at very high shell deformations.

The evolution of elastic energy that is associated with bending and stretching of the shell along with the energy stored in the microbubble due to compression of the enclosed gas, is plotted as a function of normalized deformation in Fig. 5(b). In this fashion we can compare the contribution of the different components of stiffness of the statically interrogated microbubble in the equilibrium that is achieved as the externally applied point load increases. Fig. 5(b) clearly illustrates the subdominant effect of resistance to compression of the type of polymeric microbubbles examined in the present study. Despite the fact that the internal pressure slightly increases as the shell is compressed by the external load, clearly this is not enough to render resistance to compression an important factor of the static shell response. This is also manifested by calculating the dimensionless numbers that control the microbubble response, based on equation (9), $\tilde{k}_b = 25 \cdot 10^{-6}$, $\tilde{P} = 10^{-3}$ that confirm the negligible effect of resistance to compression. This is a result of the "hard" nature of polymeric shells that, contrary to phospholipids, renders stretching and bending as the main participants of the dominant balance at equilibrium.

4. Conclusions

The response of microbubbles that are coated with a polymeric shell, subject to a static load, was investigated numerically and the results were compared against experimental data[3]. At the nanoscale, $F \leq 10$ nN, a nonlinear

regime exists in which the force balance is most likely determined by elastic and intermolecular/surface-adhesion forces. For higher applied forces, shell stretching and bending form the dominant force balance resulting in a linear regime, the Reissner regime, followed by a nonlinear regime attributed to Pogorelov. In the linear regime the shape of the microbubble is flattened in the region where the external load is applied, whereas in the nonlinear regime a crater is formed in the contact area.

The Young's modulus along with the thickness of the shell can be easily estimated from f-d curves by fitting the linear and nonlinear regimes with the asymptotic relations from Reissner's and Pogorelov's theory. The results of this methodology are in accordance with experimental values for Young's modulus and shell thickness, proving that in analogous experiments the shell thickness need not be a-priori known. This can be a very useful tool in AFM studies aiming at the mechanical characterization of coated microbubbles, whose small size and preparation procedures do not allow for reliable estimates of their shell thickness.

Numerical simulations with the finite element method, employing the elastic parameter values estimated by treating the experimental f-d curves in the above fashion, confirm the above picture but exhibit discrepancies with equivalent experimental f-d curves. Since intermolecular/surface-adhesion[6,7,8] forces are not included in the model at this point, we do not expect numerical results to reproduce the initial nonlinear regime. In addition, the point load that was used in the simulations performed here overestimates the deformation of the microbubble in the nonlinear regime of the response curve and accelerates the onset of the nonlinear Pogorelov regime. This discrepancy between experiments and simulations is understandable at high applied forces, where the contact area cannot be described with a point force, while a proper load distribution is expected to give more reliable results. In particular, when crater formation takes place around the pole of a shell subject to a point load distribution, deformation is measured exactly at the pole whereas experiments register the cantilever translation which will be smaller. It should, however, be pointed out that using the asymptotic relations provided for a point load by Reissner and Pogorelov provides quite accurate predictions of the shell parameters despite the discrepancies indicated by the simulations. This is attributed to the fact that during an actual AFM procedure a certain load distribution will exist, as opposed to a point load distribution, which is expected to decelerate buckling of the original flattened shapes. Furthermore, it has been shown by numerical studies of static shell response to a load distribution[23] that the linear Reissner regime is valid for an extended region in the response curve since higher order corrections to the Reissner response, before the response curve enters the Pogorelov regime, are negligible.

The model is currently extended to allow for a load distribution, in an effort to account for the discrepancies reported in the simulations, and to include intermolecular/surface-adhesion effects that are essential for estimating mechanical properties of the "softer" phospholipid shells.

Acknowledgments

References

1. Ferrara K, Pollard R, Borden M. Ultrasound microbubble contrast agents: Fundamentals and application to gene and drug delivery. *Annu Rev Biomed Eng* 2007;**9**:415-447.
2. Buchner Santos E, Morris J, Glynos E, Sboros V, Koutsos V. Nanomechanical properties of phospholipid microbubbles. *Langmuir* 2012;**28**:5753-5760.
3. Glynos E, Koutsos V, McDicken W, Moran C, Pye S, Ross J, et al. Nanomechanics of biocompatible hollow thin-shell polymer microspheres. *Langmuir* 2009;**25**:7514-7522.
4. Glynos E, Sboros V, Koutsos V. Polymeric thin shells: Measurement of elastic properties at the nanometer scale using atomic force microscopy. *Mater Sci Eng,B* 2009;**165**:231-234.
5. Unger E, Hersh E, Vannan M, Matsunaga T, McCreery T. Local drug and gene delivery through microbubbles. *Prog Cardiovasc Dis* 2001;**44**:45-54.
6. Johnson K, Kendall K, Roberts A. Surface energy and the contact of elastic solids. *Proc R Soc Lond A Math Phys Sci* 1971;**324**:301-313.

7. Shanahan MER. A novel test for the appraisal of solid/solid interfacial interactions. *J Adhesion* 1997;**63**:15-29.

8. Israelachvili J.N. *Intermolecular and surface forces*, 3ʳᵈ Edition: Amsterdam, 2011.

9. Reissner E. Stresses and small displacements of shallow spherical shells I and II. *J Math Phys* 1946;**25**:279-300.

10. Pogorelov A. Bendings of surfaces and stability of shells: American Mathematical Society; 1988.

11. Vella D, Ajdari A, Vaziri A, Boudaoud A. Wrinkling of pressurized elastic shells. *Phy Rev Lett* 2011;**107**:174301.

12. Lytra A, Pelekasis N, Static response and stability of coated microbubbles—multiplicity of solutions and parameter estimation. *Fluid Dyn Res* 2014;**46**:041422.

13. Timoshenko S, Woinowsky-Krieger S. *Theory of plates and shells*: McGraw-Hill; 1959.

14. Libai A, Simmonds J. *The nonlinear theory of elastic shells*: Cambridge University Press; 2005.

15. Pozrikidis C. Effect of membrane bending stiffness on the deformation of capsules in simple shear flow. *J Fluid Mech* 2001;**440**:269-291.

16. Tsiglifis K, Pelekasis N. Parametric stability and dynamic buckling of an encapsulated microbubble subject to acoustic disturbances. *Phys. Fluids (1994-present).* 2011;**23**:012102

17. Barthes-Biesel D, Diaz A, Dhenin E. Effect of constitutive laws for two-dimensional membranes on flow-induced capsule deformation. *J Fluid Mech* 2002;**460**:211-222.

18. Boor Cd. *A practical guide to splines*: Springer; 2001.

19. Pelekasis N, Tsamopoulos J, Manolis G. Equilibrium shapes and stability of charged and conducting drops. *Phys Fluids A* 1990;**2**:1328-1340.

20. Knoche S, Kierfeld J. Buckling of spherical capsules. *Phys Rev E* 2011;**84**:046608.

21. Fery A, Weinkamer R, Mechanical properties of micro- and nanocapsules: Single-capsule measurements. *Polymer.* 2007;**48**:7221-7235.

22. Ottoboni T, Tickner E, Short R, Yamamoto R. Hollow microspheres with controlled fragility for medical use. US 6776761B2, 2004.

23. Vaziri A. Mechanics of highly deformed elastic shells. *Thin Wall Struct.* 2009;**47**:692-700.